Original Article

HEALTH SCIENCES
MEDICINE

DOI: 10.32322/jhsm.1250202
J Health Sci Med 2023; 6(2): 500-505

Changes in nasolabial angle may alter nasal valve morphology and airflow: a computational fluid dynamics study

Mehmet Mustafa Erdoğan[1], Levent Uğur[2]

[1]Department of Otorhinolaryngology, Head and Neck Surgery, Sabuncuoglu Şerefeddin Training and Research Hospital, Faculty of Medicine, Amasya University, Amasya, Turkey
[2]Department of Mechanical Engineering, Faculty of Engineering, Amasya University, Amasya, Turkey

Cite this article as: Erdoğan MM, Uğur L. Changes in nasolabial angle may alter nasal valve morphology and airflow: a computational fluid dynamics study. J Health Sci Med 2023; 6(2): 500-505.

ABSTRACT

Aim: Nasal valve (NV) dysfunctions are a significant cause of nasal obstruction. Changes in the nasolabial angle (NLA) may also cause changes in NV morphology. The effect of changes in the 3D structure of the nasal valve region (NVR) on nasal airflow has yet to be studied sufficiently. The accuracy of computational fluid dynamics (CFD) simulation results of nasal airflow has been confirmed by in vitro tests. Therefore, this study aimed to evaluate the effect of changes in NV structure and volume on nasal airflow based on the CFD method.

Material and Method: We used CT images to create a 3D structural model of the NVR. First, CT images were transferred to MIMICS® software, and the nasal air passage was modeled. A solid reference model of the NVR was then created using SolidWorks software. Five different solid 3D nasal valve models were created with nasolabial angles of 85˚ in Model 1, 90˚ in Model 2, 95˚ in Model 3, 100˚ in Model 4, and 105˚ in Model 5. To simulate breathing during rest and exercise using the CFD method, the unilateral nasal airflow rates were set at 150 ml/s and 500 ml/s, respectively. The CFD method was then used to calculate each model's airflow properties. Finally, the volumes of the models, pressure at the NV outlet, and airflow velocity were evaluated and calculated to investigate each model's NV airflow characteristics.

Results: Our study found a significant correlation between the nasolabial angle (NLA) and NVR volume (r=-0.998, p=0.000), flow rate and velocity (r=0.984, p=0.000), velocity and maximum pressure (r=0.920, p=0.000), velocity and minimum pressure (r=-0.969, p=0.000), flow rate and maximum pressure (r=0.974, p=0.000), and flow rate and minimum pressure (r=-0.950, p=0.000). There was no correlation between NLA increase and nasal airflow velocity. We determined that the highest pressure and lowest airflow velocity values were in the upper angle region and that the lowest pressure and highest airflow velocity values were at the bottom of the NVR in all models.

Conclusion: Using the CFD method, we found a decrease in NVR volume and an increase in airflow velocity with an increase in NLA. In addition, we found that the pressure values in the NVR did not change significantly with the increase in NLA.

Keywords: Septorhinoplasty, nasal valve, computational fluid dynamics, nasal airflow, nasal breathing, nasolabial angle

INTRODUCTION

Nasal valve (NV) stenosis is a significant cause of nasal obstruction. NV dysfunctions have been reported to play a role in up to 13% of cases where adults suffer from nasal obstruction and 95% of cases where nasal obstruction is experienced after septoplasty (1). Even minor anatomical variations have been proven to have a significant impact on nasal airflow and related physiological functions, such as regulation of exhaled air and perception of odors (2). For this reason, patients' complaints should be listened to carefully, and the NV region (NVR) should be carefully evaluated during pre-surgical planning.

According to some authors, the NV is divided into the internal (INV) and external nasal valve (ENV). The INV is located approximately 1.3 cm behind the nostrils and is the narrowest part of the nasal airway, causing the most significant resistance to all airflow. It constitutes 50% of the total airway and approximately 70% of nasal resistance (3). Its anatomical borders are formed by the nasal septum medially, the caudal edge of the superior alar cartilage and anterior part of the inferior turbinate laterally, and the nasal floor inferiorly. The angle between the nasal septum and the

Corresponding Author: Mehmet Mustafa Erdoğan, mmerdogan2001@yahoo.com **Received:** 12.02.2023 **Accepted:** 02.03.2023

upper alar cartilage is normally 10 to 15 degrees (4). However, as an anatomical structure, the NV is not a two-dimensional cross-sectional area but a three-dimensional (3D) volumetric structure formed by many anatomical structures and cross-sectional areas. The boundaries of this 3D structure are the nostril caudally, the INV posteriorly, the alar cartilage and fibrofatty tissue anterolaterally, and the septum and medial crura medially (5). Tripathi et al. (6) opposed the division between an INV and ENV as separate structures and referred to their combination as a nasal gateway (**Figure 1**A).

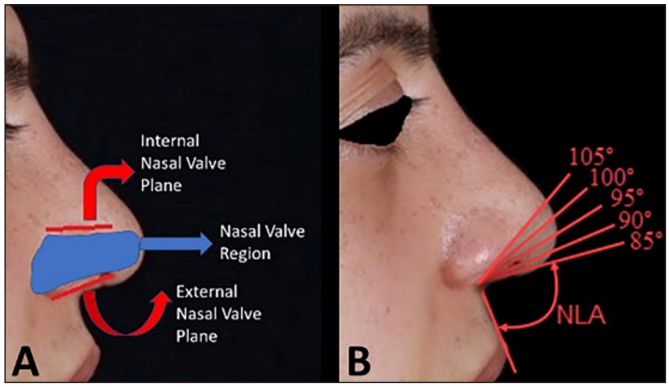

Figure 1. Nasal valve (A) and nasolabial angle (NLA) (B).

The nasolabial angle (NLA) is the angle between the base of the nose and the upper lip. This angle should be between 100–110 degrees for women and 90–105 degrees for men (**Figure 1**B) (7, 8). Changes in the NLA may cause changes in the angles and distances of the INV and ENV planes relative to each other and can change the morphology and volume of the NVR (9). However, the effect of changes in the 3D structure of the NVR on nasal airflow has not been studied sufficiently.

Computational fluid dynamics (CFD) is a discipline that combines fluid mechanics, mathematics, and computer science. CFD uses numerical simulations to analyze data on the interactions of liquids, particles, or gases whose motion is constrained by solid surfaces (10). In medicine, the results of CFD simulations are considered reliable in preoperative planning and predicting surgical outcomes, but they still require validation in real life (11, 12). In recent years, CFD has been used to predict nasal airflow and related events. The accuracy of the CFD simulation results of nasal airflow has been confirmed by in vitro experiments (13-15). CFD is low-cost, non-invasive, and makes it easier to obtain detailed results than other methods (16, 17).

This study aimed to evaluate the effect of changes in NVR structure and volume on nasal airflow based on the CFD method.

MATERIAL AND METHOD

Since our study was an experimental computer modeling, we did not receive ethics committee approval. All procedures were carried out in accordance with the ethical rules and the principles.

Model Creation

Our study used maxillofacial computed tomography (CT) images of a 33-year-old male patient with no nasal complaints to create an anatomically correct 3D structure of the NVR. CT sections were obtained using the GE Revolution CT 128-Slice (GE Healthcare, USA) with 0.625-mm thick sections in the axial plane. CT sections were analyzed using a picture archiving and communication system.

The CT images were transferred to Materialise's interactive medical image control system (MIMICS®; NV, Belgium), an interactive software program that uses CT images for visualization and segmentation operations. First, the nasal air passage was modeled in 3D using MIMICS. A threshold range of -1024 to -300 Hounsfield units (HU) was set in the air modeling, in line with previous models (18). The air passage from the nostrils to the INV was designated as the NVR. Since our aim was only to investigate the effect of the NVR on the airflow, this area was manually separated from the rest of the nasal passage, and a 3D model of the NVR was created (**Figure 2**).

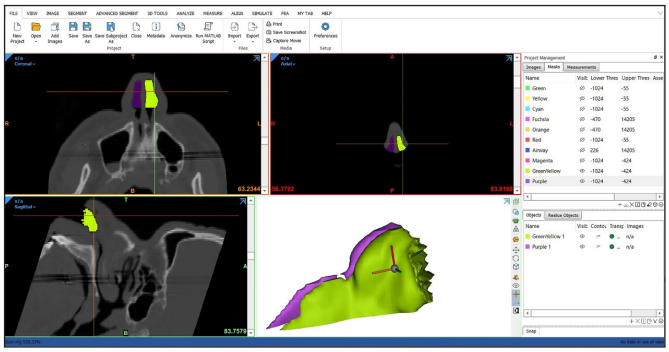

Figure 2. Creation of nasal air passage model from CT images.

The NLA was measured as 85˚ in the soft tissue measurements of the patient's CT images. The measurements obtained from MIMICS were transferred to SolidWorks (Dassault Systems), a computer-aided 3D solid modeling and design software. A solid reference model of the NVR was created with this software (**Figure 3**A). The INV and ENV cross-sections and cross-sectional areas were measured in the NVR modeled in 3D using the MIMICS program (**Figure 3**B).

As seen in **Figure 3**C, five different models were performed using the ideal NLA values in the literature by increasing the ENV plane by five degrees compared to the reference model to ensure the change in the NLA by keeping the INV plane constant on the simple reference model with an NLA of 85˚ (7). Thus, five different solid

3D NV models were created with NLAs of 85˚ in Model 1, 90˚ in Model 2, 95˚ in Model 3, 100˚ in Model 4, and 105˚ in Model 5. Using the CFD method, we then calculated the changes in airflow properties for each model.

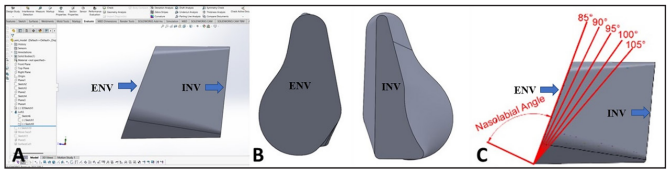

Figure 3. A. 3D creation of a simple solid model of the NVR in Solidworks. B. ENV and INV cross-sectional areas. C. Models created with NLA increments.

Numerical Method

The CFD method was used to examine the effects of changes in the NLA on airflow in the NVR, and calculations were made using ANSYS-Fluent 21.0 (ANSYS, Inc.) software (19). Since the Reynolds number calculated for the NVR input was less than 2,300, the flow was assumed to be laminar in the NVR, where all calculations were made (20, 21). Previous studies have also shown that nasal airflow is laminar in NVR (16, 22). Based on previous research, our study applied the airflow regime as a laminar flow for CFD simulations. The conservation and continuity equations used for laminar flow were as follows:

$$\rho\frac{\partial u}{\partial t}+\rho(u.\nabla)u=-\nabla p+\mu\nabla^2 u$$

$$\nabla.u=0$$

In the equations, "u" represents the air velocity vector, ρ=a 1,225-kg/m3 air density, μ=1.7894 × 10−5 kg/(m.s) dynamic viscosity of the air, p is pressure, and t is time. The SIMPLEC algorithm was used to analyze the pressure–velocity pair. The second-order method for pressure correction and the second-order UPWIND method for discretization conservation equations were used. In the time-dependent analysis, the first-order temporary closed formulation was used (23). The analyses were terminated when the residual values for the conservation of mass and momentum equations were less than 10−6. The network structure created for the calculation is shown in **Figure 4A**. The mesh structure was tetrahedral. The mesh structure was concentrated in areas close to the NV walls. A growth factor of 1.1 and bias factor of 5 were chosen near the NV walls. As seen in **Figure 4B**, when the number of grids increases above 300,000 B, the values for pressure and speed are negligible. Therefore, a grid number of 301,859 was chosen for our study.

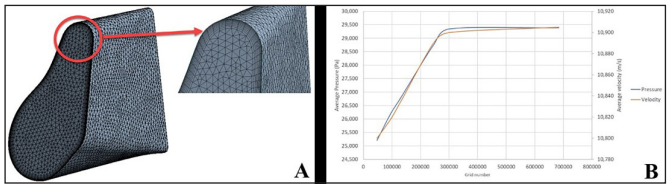

Figure 4. A. Mesh structure for NVR model. B. Grid independence test.

The velocity inlet boundary condition is given at the entrance of the calculation region, and the outflow boundary condition is given because the pressure value cannot be estimated at the outlet. In the NVR, the inner walls were considered rigid, and the no-slip velocity condition (u=0) was assigned. An inlet pressure boundary condition with zero-gauge pressure was applied in the nostril. To simulate breathing during rest and exercise in the CFD method, the airflow rates passing through the nostril section were set in previous studies as 150 ml/s in the resting state for the single nasal passage and 500 ml/s in the exercise state (13, 16, 18, 24). To provide these flow rates, the inlet pressure in the nostril was accepted as the atmospheric pressure, and the outlet pressure was adjusted. Parameters such as the pressure at the NV outlet and airflow rate were then calculated to determine the NVR's airflow characteristics.

Statistical Analysis

All data were analyzed using the Statistical Package for the Social Sciences (SPSS) (IBM) version 25 software. The Pearson Correlation test was used to evaluate the correlation between the data obtained from the NVR models. Values with a "p" value below 0.05 were considered significant for correlation.

RESULTS

The data from the experimental NVR models and the pressure and velocity results obtained from the study are shown in **Table 1** and **Figure 5**.

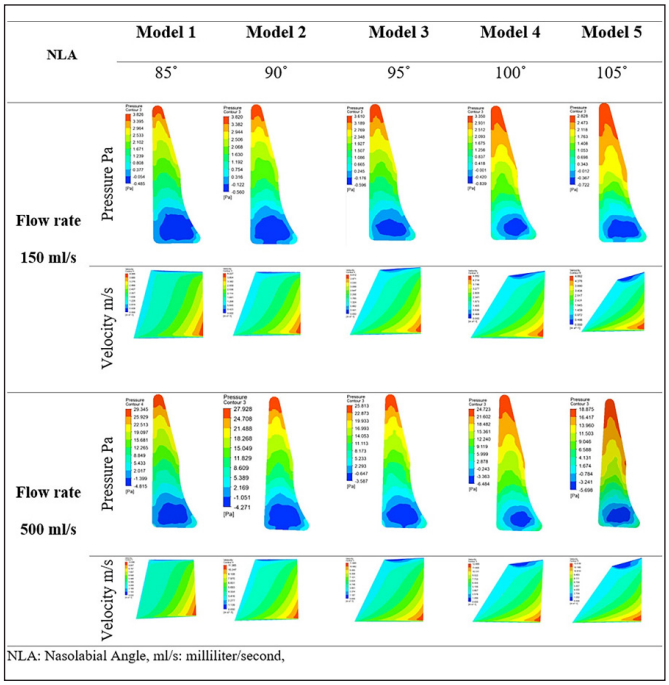

Figure 5: Cross-sectional velocity contours and pressure patterns of the nasal airflow at flow rates of 150 ml/s and 500 ml/s.

Table 1. Data obtained from models and pressure and velocity values.

NLA	Model 1	Model 2	Model 3	Model 4	Model 5
	85˚	90˚	95˚	100˚	105˚
150 ml/s					
Max.Pressure (Pa)	3.83	3.82	3.61	3.35	2.83
Min.Pressure (Pa)	-0.49	-0.56	-0.6	-0.84	-0.72
Velocity (m/s)	4.1	4.23	4.41	4.68	4.86
500 ml/s					
Max.Pressure (Pa)	29.35	27.93	25.81	24.72	18.88
Min.Pressure (Pa)	-4.82	-4.27	-3.59	-6.48	-5.7
Velocity (m/s)	11	11.39	11.87	12.89	13.52
Angle between INV–ENV planes	15˚	20˚	25˚	30˚	35˚
Volume (mm^3)	5,575	5,267	4,908	4,506	4,071
Mesh numbers	301,859	287,412	270,690	250,726	229,548

NLA: Nasolabial Angle, Max.:Maximum, Min.: Minimum, ml/s: milliliter/second, Pa: Pascal,

The NVR volume in the generated 3D NV models decreased as NLA increased. While the volume was 5574.9 mm^3 in Model 1, it was 4070.7 mm^3 in Model 5. The angle between the INV and ENV planes increased as the NLA increased. The Pearson correlation (r) and p values of the data are given in **Table 2**.

Table 2. Pearson correlation values (r) between variables.

	Max. Pressure	Min. Pressure	Velocity	Volume
Flow rate	0.974*	-0.950*	0.984*	0.000
NLA	-0.168	-0.119	0.154	-0.998*
Max. Pressure		-0.891*	0.920*	0.170
Min. Pressure			-0.969*	0.125
Velocity				-0.155

NLA: Nasolabial angle, Max.: Maximum, Min.: Minimum, *p < 0.001

DISCUSSION

Nasal breathing has multiple functions and is essential for maintaining a good quality of life. The geometry of the nose, which provides the physical boundary condition of healthy breathing, is highly complex. The NVR is generally defined anatomically as the region of the nasal cavity that offers the most significant resistance to airflow. Therefore, it is the most critical region for nasal airflow (25). Even the slightest change in the NVR can substantially affect airflow within the nasal cavity (11). Garcia et al. (26) confirmed that anterior septal deviation, including in the NVR, increases nasal resistance more than median and posterior deviations. Small changes in the NLA significantly affect patient satisfaction aesthetically (27, 28). However, there will inevitably be a change in the NVR, a 3D structure, when increasing or decreasing the nasal tip rotation with the methods applied during nasal-type surgery.

The primary purpose of nasal surgery is to provide the patient with a functional nose that breathes well. However, if adequate airflow cannot be achieved after the surgery, patients may complain of shortness of breath, and even an aesthetically pleasing nose will not necessarily satisfy the patient functionally (29).

The perception of nasal airflow is a subjective sensation; therefore, it is difficult to determine its amount and possible causes of obstruction. For objective measurements of nasal obstruction, tests such as rhinomanometry, acoustic rhinometry, peak nasal inspiratory flow, and laser doppler anemometry can be used in the clinic. However, the results of these tests are weakly associated with subjective nasal obstruction. Therefore, they have not entered into routine clinical use because their clinical value is controversial and the cost of testing is high (11, 12, 18, 30).

In recent years, CFD has been a generally accepted and clinically correlated method for evaluating nasal airflow (31). Zhu et al. (13), in their study using CFD, determined that a curved external nose created greater nasal resistance in the nasal passage than the normal situation. In contrast, nasal passage stenosis caused by turbinate hypertrophy increased resistance even more. The effects of septal deviation and atrophic rhinitis in the nasal cavity on nasal airflow have also been reported by CFD studies (26). Nasal functions, such as nasal airflow structures and heating capacity, were also numerically evaluated using CFD (13).

In our study, we examined the effect of changes in the 3D structure of the NVR on nasal airflow by designing a solid model using the CFD method. Borogeni et al. (18) reported that subjective nasal airflow scores were more compatible with unilateral CFD results than bilateral results. In addition, Andre et al. (12) found that nasal airflow perception was better associated with unilateral airflow. For these reasons, we used unilateral nasal modeling.

To evaluate the airflow characteristics in the NVR, the airflow velocity and the pressure at the NVR outlet are essential indicators (31). We evaluated these two parameters in our study.

According to Bernoulli's principle, the airflow velocity and pressure will increase when the nasal cavity narrows (31). The narrowing of the nasal passage causes an increase in airflow velocity (13). From this point of view, an increase in the volume of the NVR will slow down the airflow, while a decrease in the volume will increase the speed. In our study, as the NLA increased, the volume decreased in the NVR models, and the airflow velocity increased in line with the literature (18, 25). However, there was no correlation detected between the NLA

and nasal airflow velocity. This is probably because our study was performed on a single anatomical model, with few angle models and flow rates of only 150 ml/s and 500 ml/s. With more modeling, statistical data with more evidence could be obtained. There was a very high negative correlation between NLA and volume, which was statistically significant (p=0.000). We also found a very high positive correlation between nasal flow rate and airflow velocity, which was statistically significant (p=0.000). Similarly, we found a very high positive correlation between nasal airflow velocity and maximum pressure and a very high negative correlation between nasal airflow velocity and minimum pressure at the NV outlet, both of which were statistically significant (p=0.000), (p=0.000). Finally, there was a strong positive correlation between flow rate and maximum pressure and between flow rate and velocity, and a negative correlation between flow rate and minimum pressure. All these correlations were statistically significant (p=0.000), (p=0.000), (p=0.000).

The pressure values at the NV outlet are essential parameters for nasal airflow evaluation (32). Changes in nasal passage anatomy may also cause changes in pressure values. For example, in their CFD study, Zhao et al. (21) found that the INV was the narrowest cross-sectional area of the entire nasal airway, and 50%–73% of the entire nasal airway pressure drop was in the NVR. In the same study, pressure changes were detected at the highest value in the NVR and were compatible with clinical tests and scoring (21). Our study found that all models' maximum pressure values at the NV outlet decreased as the NLA increased. However, no correlation was detected. Moreover, no correlation was detected between NLA increase and minimum pressure. We found that as the NLA increased, the maximum pressure values increased at an airflow of 500 ml/s, but the minimum pressure values decreased to 95˚, then increased to 100˚ NLA, and decreased to 105˚ NLA again. In the evaluation made with a 500-ml/s flow rate, we think that the fluctuation of the minimum pressure values at the NV outlet, diverging from the values with a 150-ml/s flow rate, is most likely due to the possibility of the airflow passing from a laminar to turbulent flow in this region due to high velocity (11).

As a result of the evaluation of the NVR with CFD, we determined that the highest pressure values were in the upper angle region, which is the narrowest part of the NVR. The nasal airflow velocity values in this region were the lowest. On the contrary, we found the lowest pressure and highest airflow velocity values at the bottom of the NVR in all models. Similar to Li et al. (17), our study determined that the peak airflow velocity was located in the lower part of the NVR in all models.

Limitations

The limitation of our study was that it was an isolated experimental study in which only the NVR was examined out of the entire nasal passage, and only a few parameters were studied using a single anatomical model.

CONCLUSION

In our study, which used the CFD method, we found a decrease in NVR volume and an increase in airflow velocity with an increase in NLA. In addition, we found that the pressure values in the NVR did not change significantly with the increase in NLA.

Primary data may have been obtained in our study, and it shows the efficacy of the CFD method. However, in the future, more studies in which the entire nasal passage is modeled, and supported by relevant clinical data could be obtained with higher levels of evidence.

ETHICAL DECLARATIONS

Ethics Committee Approval: Since our study was an experimental computer modeling, we did not receive ethics committee approval.

Informed Consent: Since our study was an experimental computer modeling, no written informed consent form was obtained from patient.

Referee Evaluation Process: Externally peer-reviewed.

Conflict of Interest Statement: The authors have no conflicts of interest to declare.

Financial Disclosure: The authors declared that this study has received no financial support.

Author Contributions: All of the authors declare that they have all participated in the design, execution, and analysis of the paper, and that they have approved the final version.

Acknowledgement: The authors thank Prof. Dr. Mehmet Topal for his contributions to statistical evaluations.

REFERENCES

1. Barrett DM, Casanueva FJ, Cook TA. Management of the Nasal Valve. Facial Plast Surg Clin North Am 2016; 24: 219-34.
2. Schriever VA, Hummel T, Lundstrom JN, Freiherr J. Size of nostril opening as a measure of intranasal volume. Physiol Behav 2013; 110-111: 3-5.
3. Farina R, Gonzalez A, Toledo X, Villanueva R, Martinez B, Perez H. Relationship between nostril, nasal valve and minimal cross-sectional area in functional upper airway. J Craniofac Surg 2019; 30: 2202-6.
4. Gelardi M, Ciprandi G. The clinical importance of the nasal valve. Acta Biomed 2019; 90: 31-3.
5. Hamilton GS, 3rd. The external nasal valve. Facial Plast Surg Clin North Am 2017; 25: 179-94.
6. Tripathi PB, Elghobashi S, Wong BJF. The myth of the internal nasal valve. JAMA Facial Plast Surg 2017; 19: 253-4.

7. Armijo BS, Brown M, Guyuron B. Defining the ideal nasolabial angle. Plast Reconstr Surg 2012; 129: 759-64.
8. Harris R, Nagarkar P, Amirlak B. Varied definitions of nasolabial angle: searching for consensus among rhinoplasty surgeons and an algorithm for selecting the ideal method. Plast Reconstr Surg Glob Open 2016; 4: e752.
9. Doorly DJ, Taylor DJ, Gambaruto AM, Schroter RC, Tolley N. Nasal architecture: form and flow. Philos Trans A Math Phys Eng Sci 2008; 366: 3225-46.
10. Leite SHP, Jain R, Douglas RG. The clinical implications of computerised fluid dynamic modelling in rhinology. Rhinology 2019; 57: 2-9.
11. Berger M, Pillei M, Mehrle A, et al. Nasal cavity airflow: Comparing laser doppler anemometry and computational fluid dynamic simulations. Respir Physiol Neurobiol 2021; 283: 103533.
12. André RF, Vuyk HD, Ahmed A, Graamans K, Nolst Trenité GJ. Correlation between subjective and objective evaluation of the nasal airway. A systematic review of the highest level of evidence. Clin Otolaryngol 2009; 34: 518-25.
13. Zhu JH, Lee HP, Lim KM, Lee SJ, San LT, Wang de Y. Inspirational airflow patterns in deviated noses: a numerical study. Comput Methods Biomech Biomed Engin 2013; 16: 1298-306.
14. Segal RA, Kepler GM, Kimbell JS. Effects of differences in nasal anatomy on airflow distribution: a comparison of four individuals at rest. Ann Biomed Eng 2008; 36: 1870-82.
15. Radulesco T, Meister L, Bouchet G, et al. Correlations between computational fluid dynamics and clinical evaluation of nasal airway obstruction due to septal deviation: An observational study. Clin Otolaryngol 2019; 44: 603-11.
16. Li C, Jiang J, Dong H, Zhao K. Computational modeling and validation of human nasal airflow under various breathing conditions. J Biomech 2017; 64: 59-68.
17. Li L, London NR, Jr., Zang H, Han D. Impact of posterior septum resection on nasal airflow pattern and warming function. Acta Otolaryngol 2020; 140: 51-7.
18. Borojeni AAT, Garcia GJM, Moghaddam MG, et al. Normative ranges of nasal airflow variables in healthy adults. Int J Comput Assist Radiol Surg 2020; 15: 87-98.
19. Ansys I. ANSYS fluent user's guide, release 19.0. ANSYS Inc, Canonsburg. 2018.
20. Sharp KV, Adrian RJ. Transition from laminar to turbulent flow in liquid filled microtubes. Experiments in Fluids 2004; 36: 741-7.
21. Zhao K, Jiang J. What is normal nasal airflow? A computational study of 22 healthy adults. Int Forum Allergy Rhinol 2014; 4: 435-46.
22. Kelly J, Prasad A, Wexler A. Detailed flow patterns in the nasal cavity. J Appl Physiol 2000; 89: 323-37.
23. Keskin G, Kaya AT. Evaluation of the pressure and wall shear stress on the aneurysm wall according to the growth position of a femoral artery pseudoaneurysm by numerical analysis. Eur J Sci Technol 2022; 34: 800-4.
24. Naughton JP, Lee AY, Ramos E, Wootton D, Stupak HD. Effect of nasal valve shape on downstream volume, airflow, and pressure drop: importance of the nasal valve revisited. Ann Otol Rhinol Laryngol 2018; 127: 745-53.
25. Rhee JS, Weaver EM, Park SS, et al. Clinical consensus statement: Diagnosis and management of nasal valve compromise. Otolaryngol Head Neck Surg 2010; 143: 48-59.
26. Garcia GJM, Rhee JS, Senior BA, Kimbell JS. Septal Deviation and Nasal Resistance: An Investigation using Virtual Surgery and Computational Fluid Dynamics. Am J Rhinol Allergy 2010; 24: 46-53.
27. Bucher S, Kunz S, Deggeller M, Holzmann D, Soyka MB. Open rhinoplasty using a columellar strut: Effects of the graft on nasal tip projection and rotation. Eur Arch Otorhinolaryngol 2020; 277: 1371-7.
28. Rho NK, Park JY, Youn CS, Lee SK, Kim HS. Early changes in facial profile following structured filler rhinoplasty: an anthropometric analysis using a 3-dimensional imaging system. Dermatol Surg 2017; 43: 255-63.
29. Hsu DW, Suh JD. Anatomy and physiology of nasal obstruction. Otolaryngol Clin North Am 2018; 51: 853-65.
30. Gagnieur P, Fieux M, Louis B, Bequignon E, Bartier S, Vertu-Ciolino D. Objective diagnosis of internal nasal valve collapse by four-phase rhinomanometry. Laryngoscope Investig Otolaryngol 2022; 7: 388-94.
31. Li L, Han D, Zang H, London NR. Aerodynamics analysis of the impact of nasal surgery on patients with obstructive sleep apnea and nasal obstruction. ORL J Otorhinolaryngol Relat Spec 2022; 84: 62-9.
32. Zhou B, Huang Q, Cui S, Liu Y, Han D. Impact of airflow communication between nasal cavities on nasal ventilation. ORL J Otorhinolaryngol Relat Spec 2013; 75: 301-8.